Final Report

Microwave-Assisted Green Solvolysis of Wind Turbine Blades for Upcycling into Photoluminescent Safety Tiles

Humay Hamidli, Gozal Humbatzada, Hasan Babayev, Nigar Baghirzade, Muntaha Shaikh

Institution:
Ulm University
Institute of Chemical Engineering

Supervisor:
Hannes Stagge, M.Sc.

Lecturer in charge:
Prof. Dr.-Ing. Robert Güttel

25.07.2025

Table of Contents

1. Introduction

With the glow that guides, the clarion that saves: Glarion lights the way to safety.

Decommissioned wind turbines are producing vast quantities of composite waste, primarily glass fiber-reinforced plastic. Due to this materials content, traditional disposal methods like landfilling are unsustainable which is already banned. The majority of the existing recycling techniques are considered to be inadequate due to drawbacks like high energy consumption and fiber degradation [1]. In contrast, solvolysis offers a cleaner, circular approach. It uses solvents to dissolve resins while preserving fibers and enabling chemical recovery, with minimal emissions when powered by renewable energy.

Figure 1. Final Product: High-Performance Photoluminescent Safety Tile.

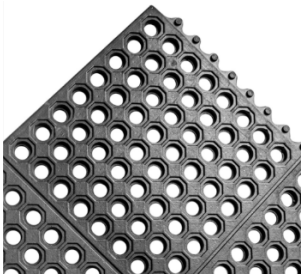

Figure 2. Final Product: Rubber Floor Block.

This project proposes converting blades into photoluminescent safety tiles (see Figure 1.) [2] and rubber floor blocks (see Figure 2.) [3] via microwave-assisted solvolysis with green solvent. The safety tiles, used in industrial settings to mark emergency exits and hazardous zones, are fire-resistant, slip-safe, and reusable, ideal for infrastructure with the critical risk of incidents. The rubber floor block, developed for industrial plants, ensures long-term user safety, even changing wet or dry conditions. These solutions turn structural waste into sustainable safety products and this project will explore how it can actually happen.

2. Literature Review

Several strategies for managing Glass Fiber Reinforced Polymer (GFRP) waste have been investigated, each with advantages and limitations. These methods can be categorized into mechanical, thermal, and chemical recycling. While mechanical recycling is simple and cost-effective, it was not chosen because of formation of low-value products. Thermal recycling demands high energy. At the end, chemical recycling, especially solvolysis is selected over the other methods as it can recover high quality fibers and resin components.

Oliveux et al. [4] established a foundational approach using conventional heating to degrade a model epoxy resin. They enhanced degradation by using greener solvent systems, such as CO_2-expanded water and mixtures of water with acetone. CO_2-expanded water is formed by dissolving pressurized CO_2 into water, which reduces the viscosity and enhances mass transfer. An 80% acetone-water mixture achieved 93% resin degradation, but the process remained slow (30-60 minutes) and required high temperatures (350°C) and pressures [4].

Rani et al. [5] shifted the focus by using a Microwave-Assisted Chemical Recycling (MACR) process. As a solvent they used hydrogen peroxide and acetic acid. They achieved over 97% epoxy degradation in an unprecedented 180 seconds. The key to this efficiency is the microwave's rapid, volumetric heating, which generates highly reactive radicals. That decompose the matrix without thermally damaging the fibers by retaining 99.8% of their original tensile strength [5].

In chemical recycling of epoxy composites, hydrogen peroxide (H_2O_2) acts as a strong oxidizing agent, while acetic acid (CH_3COOH) functions as a mild acid and solvent, and together they form peracetic acid (CH_3COOOH) in situ (8), which decomposes under microwave heating to generate highly reactive acyloxy (3) and hydroxyl (2) radicals that break down the epoxy network by cleaving C–N and other bonds, leading to the disintegration of the cured resin and release of the embedded fibers (see Figure 3. [5]).

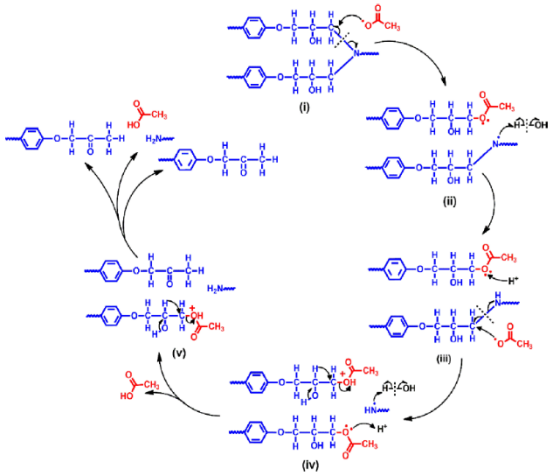

Figure 3. Plausible reaction mechanism for the disintegration of the epoxy framework

$$CH_3COOH + H_2O_2 \rightleftharpoons CH_3COOOH + H_2O \quad (1)$$

$$CH_3COOOH \rightarrow CH_3COO\bullet + \bullet OH \quad (2)$$

$$CH_3COOOH + \bullet OH \rightarrow CH_3COO\bullet + H_2O \quad (3)$$

$$CH_3COOOH + \bullet OH \rightarrow CH_3CO\bullet + O_2 + H_2O \quad (4)$$

$$CH_3COO\bullet \rightarrow \bullet CH_3 + CO_2 \quad (5)$$

$$2CH_3COO\bullet \rightarrow 2\bullet CH_3 + CO + O_2 \quad (6)$$

$$\bullet CH_3 + O_2 \rightarrow CH_3COO\bullet \quad (7)$$

$$CH_3COO\bullet + \bullet OH \rightarrow CH_3COOOH \quad (8)$$

Although the lab experiments on the literature show promising results [4], modular scale-out microwave-assisted solvolysis poses challenges such as material selection, reactor control, process safety that this project will explore.

3. Process Concept and Design

3.1 Process Description

Node 1: Feedstock Pre-Treatment & Solvolysis Reaction (100-Series)

The initial stages are the preparation of raw materials and the core chemical reaction. The process commences with the pre-treatment of wind turbine blades. The blade segments collected in the storage (1 m × 1 m × 10 cm) go through manual removal of wood and Magnetic Separation (AT-101) of metals. This mechanical size-reducing step shreds the blades into smaller, more manageable pieces, increasing the surface area for the solvolysis and easy handling. The resulting shredded material (LL-104) is conveyed to Powder Silos. A solvent solution is prepared in a Mixing Tank (AM-101) by combining Hydrogen Peroxide, Acetic Acid, and Water. The prepared solvent is pre-heated in a Heater with a combined hot water stream (AC-101) before being introduced into the reaction system (LL-128). Shredded blade material is metered from the storage silos and combined into a single feed stream (LL-109). Both the shredded material and the hot solvent are fed into a parallel of four series Solvolysis Reactors (RE-101 to RE-104). Inside the reactors, the slurry is

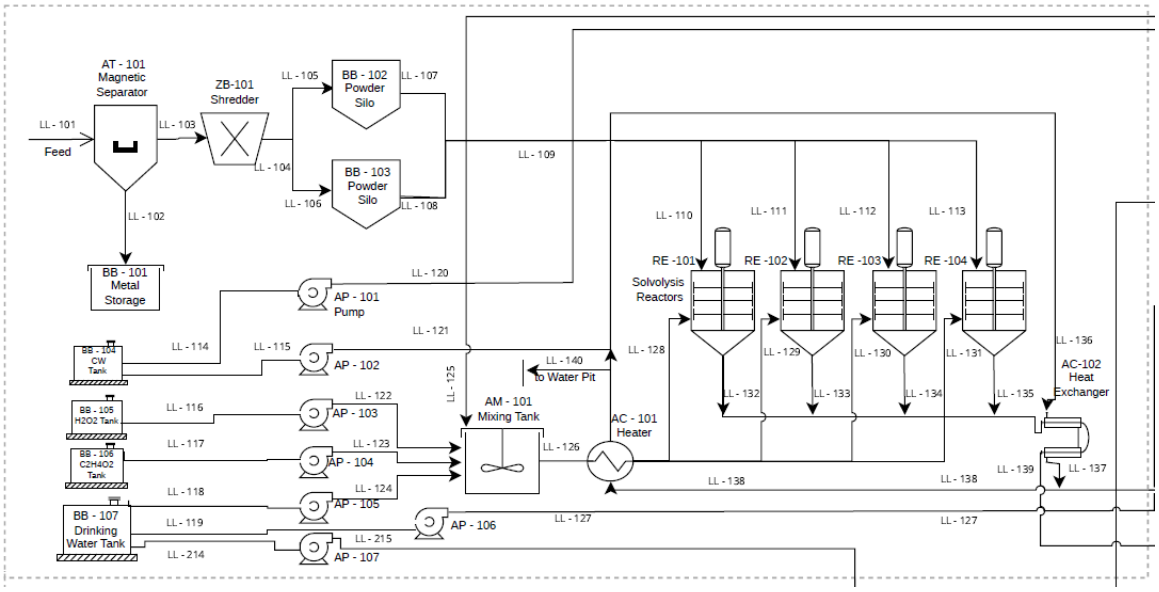

Figure 4. Process Flow Diagram Node 1.

maintained at 90 °C under atmospheric pressure. The residence time is 3 hours. The agitator is scraper with very large and long internals reaching near the walls and taking all the potential collection of the matrix and avoiding the sticking of the matrix to the walls. Microwave-assisted heating ensures uniform temperature control, while agitators keep the solids suspended. The acidic environment dissolves the resin, leaving the glass fiber matrix structurally undamaged. The slurry flows sequentially through the reactors, exiting the final reactor as stream LL-135. This stream is then cooled in a Heat Exchanger (AC-102) before being sent to the separation stage. During the solvent preparation, depending on the solvent solution composition, required amount of solution components is dosed from the fresh supply under the ratio controls (see Figure 4.).

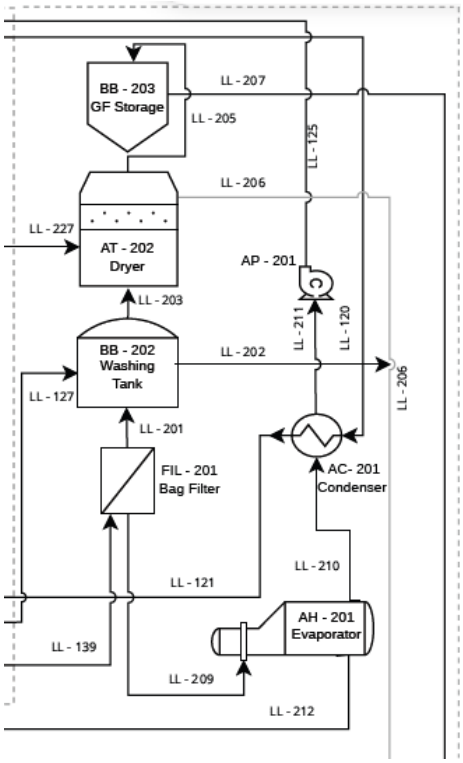

Figure 5. Process Flow Diagram Node 2.1.

Node 2: Solid-Liquid Separation & Material Recovery (200-Series)

This stage separates the solid glass fibers from the liquid resin matrix and solvent solution.

The cooled slurry from the reaction stage enters via LL-139 the Bag Filter (FIL-201). In the washing tank, the solid glass fibers are washed. The recovered wet fibers are then transferred to the Dryer. The final dried glass fibers are sent to Glass Fiber (GF) Storage (BB-203), from which they sent to product formation (LL-207).

The liquid phase, containing dissolved resin and solvent, filtered out from the Bag Filter is fed into the Evaporator (AH-201). Here, the volatile solvent is vaporized (LL-209), then re-condensed in the Condenser (AC-201) (see Figure 5) and recycled back to the Mixing Tank (AM-101). The wastewater from the Washing Tank sent to the Wastewater Pit. The resin matrix and unrecovered solvent are discharged

from the bottom of the evaporator via LL-212 to be neutralized with the NaOH in Figure 6. After that it enters to

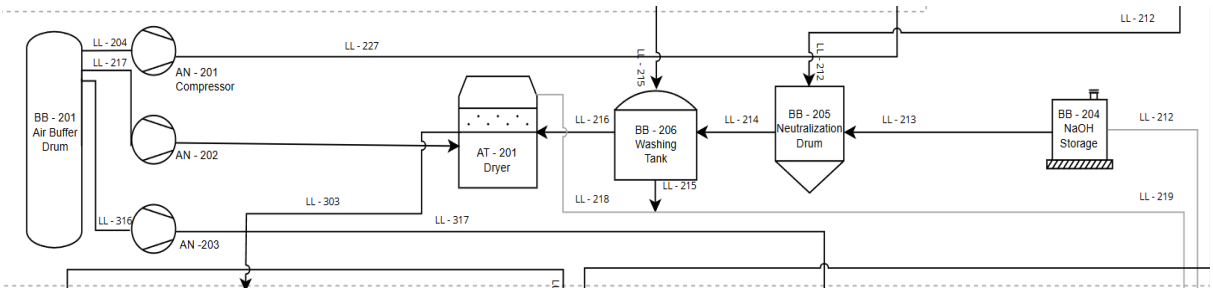

Figure 6. Process Flow Diagram Node 2.2.

the Washing Tank (BB-206) to remove the salts and unnaturalized acids and then the moisture is removed with air in the Dryer (AT-201).

Node 3: Final Product Formation (300-Series)

This final stage combines recovered and new materials to create value-added products. The process begins with curing in the reactor. The thermoplastic matrix together with hardener from Storage (BB-303) are fed in the Curing Reactor (RE-301). Curing is performed at 80 °C for 2 h followed by post-curing at 120 °C for 1 h. Curing hardens the matrix by forming crosslinks between chains, giving the material strength, thermal stability, and durability needed for structural applications. The process enables to get to a usable and stable resin matrix using a Recyclamine hardener in curing,

whose cleavable acetal/ketal groups are key to its breakdown in mild acid [5],[6]. This transformation occurs through crosslinking reactions, initiated by heat and a curing agent. It's what transforms a reactive resin into a high-performance, moldable material, making the reuse of recycled epoxy viable for structural or safety-related applications.

Wood from Storage is shredded and transferred via stream LL-309 and an Additive Package (PK-304) is added to the to a Mixing Silo. In the silo, these components are thoroughly blended with the glass fiber and cured matrix to form a composite compound. From this silo, the compound is transferred to two parallel Molder units, where it is shaped into safety tiles and rubber blocks. The molded tiles are sent to a final Air Cooler (AC-301). The cooled product is sent to Product Storage. Finally, the products are sent to the Packing station for dispatch (see Figure 7.).

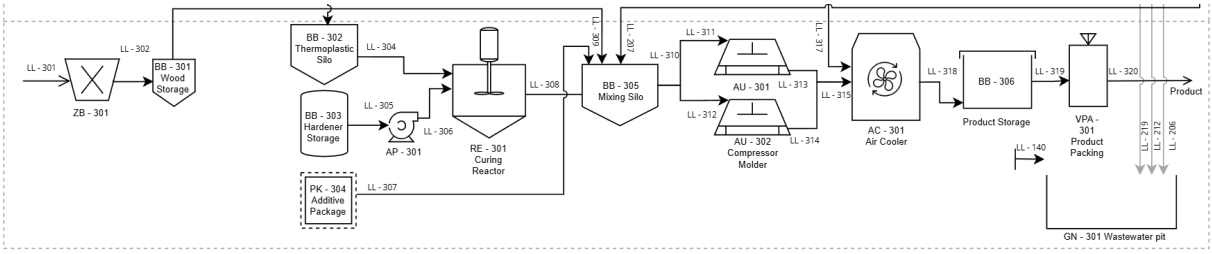

Figure 7. Process Flow Diagram Node 3.

3.2 Process Flow and Instrumentation (P&ID)

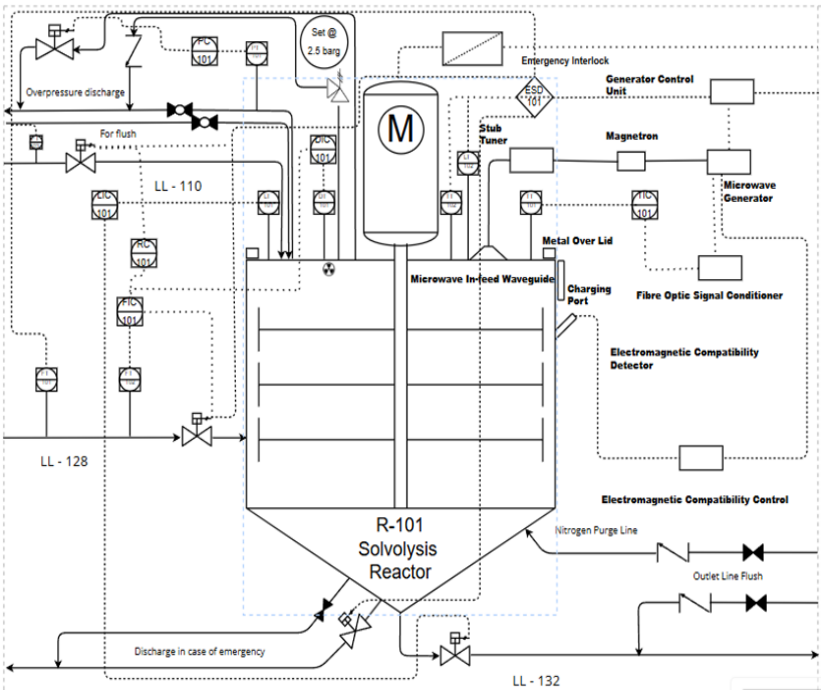

Figure 8. Process and Instrumentation Diagram of Solvolysis Reactor.

The reactor material is chosen to be Teflon according to [6].The system is designed for batch operation and features a top-mounted motorized agitator to ensure homogeneous mixing, heat distribution and wall sweeping as the blades reach near the walls (relatively low rpms). Solvent and composite input are equipped with flow and ratio controller to support precise dosing and process monitoring. To ensure material consistency and process reliability, a DIC (Density Controller with radioactive sensor) is used to monitor and control the slurry density inside the reactor by manipulating the solvent solution inlet to the reactor. The reactor is heated by a microwave system consisting of a magnetron, stub tuner, and waveguide, which delivers high-frequency energy directly into the reactor through a dedicated inlet. Emergency Shutdown (ESD-101) interlock is in place to halt microwave input and flows to the reactor case of unsafe conditions (see Figure 8.).

Together with safety and utility features (nitrogen purge, safe emergency discharge to blowdown unit), the reactor and its control systems enable efficient and reliable microwave-assisted solvolysis under tightly regulated conditions.

3.3 Raw Materials and Products

Compositional analysis from sources like Johst et al. [7], shows that while the primary targets for this recycling process are the epoxy resin and its GFRP, the feedstock contains significant amounts of other materials. These include wood cores, metals from the blade root and lightning protection system, and polymers such as PVC and PUR foams. The process acknowledges this complexity; initial pre-treatment stages separate bulk wood and metals, preparing cleaner composite feed for chemical reaction.

The aqueous solution of Acetic Acid with Hydrogen Peroxide as a solvent was chosen for its favorable environmental and chemical properties. It is biodegradable, non-toxic, and effective at breaking down the targeted resin at mild operating temperatures, an advantage over more aggressive methods [8]. The assumption that recovered solvent can be reused as fresh is non-trivial and requires chemical justification. Reactive intermediates such as peracetic acid and free radicals are generated and consumed during epoxy degradation, potentially altering the solvent's oxidative potential. Nevertheless, if the post-reaction solvent composition is analytically monitored and the concentrations of active constituents are restored to optimal levels, the solvent system can be effectively regenerated and reused without compromising the degradation efficiency.

To transform the recovered materials into a high-performance safety tile, 9 specialized additives are incorporated during the final compounding stage. Each component is selected to a specific, critical function. To meet European fire safety norms like EN 13501-1, halogen-free flame-retardant system is used. This system combines DOPO, an organophosphorus compound that acts in the gas phase to interrupt combustion, with Aluminum Oxide and Zinc Borate, which work in the solid phase to form a protective, insulating char layer [9]. The tile's signature "glow-in-the-dark" safety feature uses a phosphorescent pigment: Strontium Aluminate doped with Europium and Dysprosium ($SrAl_2O_4$:Eu,Dy) [10]. This material is the industry standard for professional

safety applications due to its high initial brightness and a long afterglow, ensuring visibility after power failure. Long-term durability is achieved through stabilizers. A Hindered Amine Light Stabilizer (HALS) protects the polymer from UV degradation[11], while the antioxidant Irganox 1010 prevents thermal breakdown during molding and over the product's service life [12]. A Maleic Anhydride Grafted Polypropylene (MAH-g-PP) acts as a coupling agent. This molecule functions as a chemical bridge, creating a strong bond between the inorganic glass fiber surfaces and the organic polyurethane matrix. This enhanced adhesion is essential for the high (60%) recycled fiber content to achieve excellent mechanical strength [13].

The primary product is a durable, photoluminescent, fire-retardant safety tile developed for demanding industrial applications especially for the plants designed vertically to save the space. The second product blocks floor blocks are ideal for the safety of the personnel for accessing the facilities in the pavements of power stations, terminals and other industrial facilities.

3.4 Utilities and Auxiliary Units

Compressed air system is essential for both automation and material transport. This system is composed of three Compressors (AN-201, AN-202, AN-203) in Figure 5, that feed a central Air Drum (BB-201). This drum acts as a receiver to buffer the air supply and reduce pressure fluctuations.

The reactor operates adiabatically. The cooling water is used to cool down the reactor effluent temperature to 70 °C in order to prevent the further degradability and plugging of the pipes. Nitrogen is used for purging, inertization and blanketing purposes.

To comply with environmental regulations, all liquid effluent from the plant is collected. The primary collection point for this is the Wastewater pit (GN-301). This system collects waste process water, wash water, and other aqueous streams. Due to the acidity in the process, caustic soda, is added to adjust the pH to a neutral range before the treated water is sent to a service company for further treatment.

Ferrous metal parts are recovered by the Magnetic Separator (AT-101) are collected and given for metal recycle. Other solid wastes, including used filter media, off-spec product, and general plant refuse, are collected in designated areas and disposed of according to local regulations or sold for cheaper low- quality-grade applications. A stable green electrical supply is crucial for all for the reactors, rotating equipment like pumps and compressors, as well as for instrumentation.

3.5 Process Design and Capacity

The proposed recycling plant will be located in Wilhelmshaven, a strategic port city in Lower Saxony, Germany. This site was chosen for its supply of wind turbine blades and its industrial infrastructure for distributing the final products [8]. The diagram (see Figure 9) shows, the ideal annual production capacity of the microwave-assisted solvolysis plant designed to recycle

decommissioned wind turbine blades into photoluminescent safety tiles can be seen. The process operates in semi-batch mode with four parallel reactors. Each total batch, representing the combined output from all reactors, processes initial charge of 2242 kilograms of composite feedstock (after Wood Removal and Metal Separation) and 1167 kilograms of solvent solution. During solid-liquid separation, 1389 kilograms of glass fiber are fully recovered in the bag filter. In the solvent separation unit, 997 kilograms of solvent are recovered, filtered from mechanical particles, and recycled into the solvent mixing tank. The balance is done for steady state, with hydrogen peroxide, acetic acid, and drinking water added as needed based on the solvent composition.

Following the curing stage, the recovered glass fiber is compounded with a thermoplastic matrix, additives, and wood filler. This mixture is molded into high-performance safety tiles. Each full batch yields an ideal output of 2397 kilograms of final product.

The batch cycle consists of 3 hours of reaction time and an hour for discharge, flushing, and charging, totaling 4 hours. With six complete batches processed per day across the four reactors, and 330 operational days per year, the facility executes 1980 batches annually.

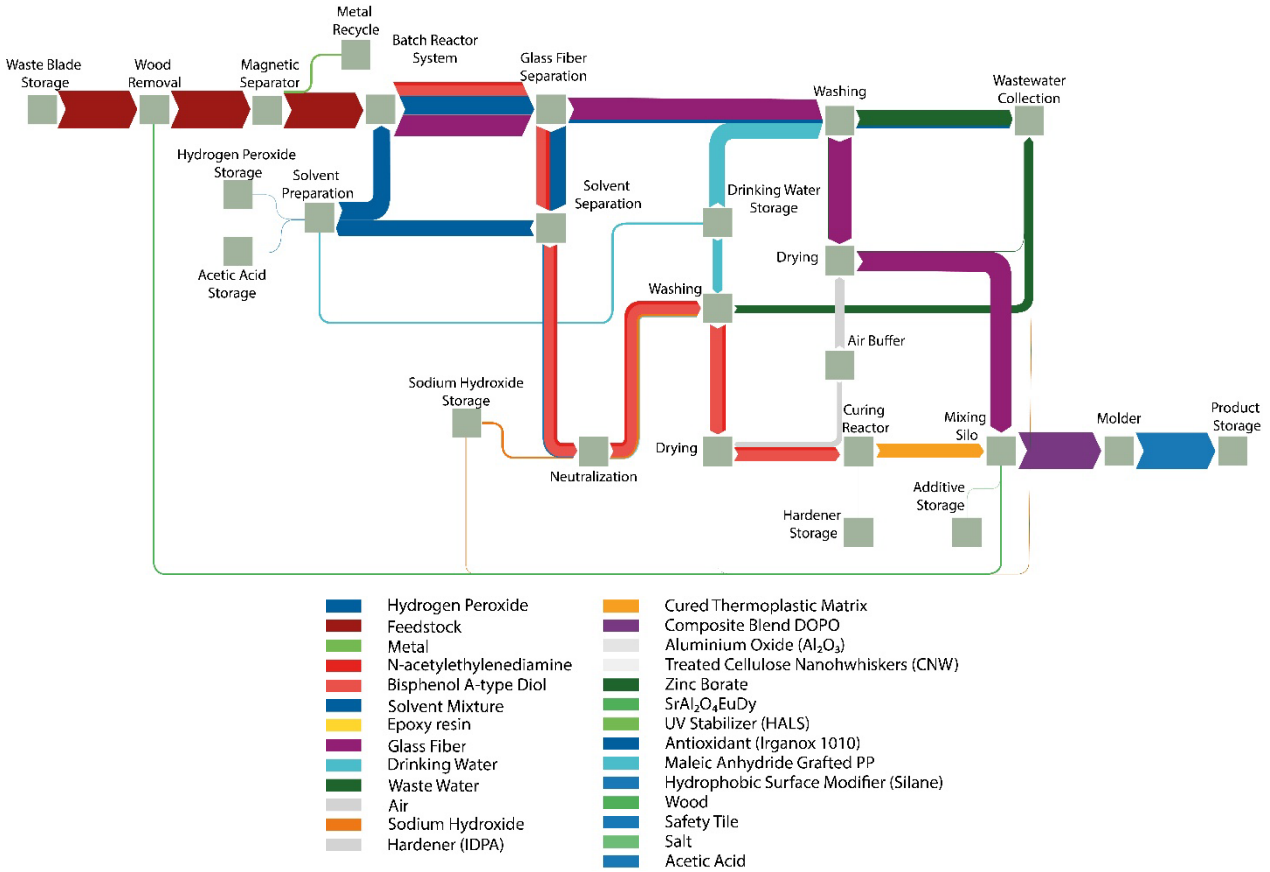

Figure 9. Process Schematic for the Solvolysis of Composite Blade Waste.

Under these conditions, the plant processes approximately 4438 tonnes of feedstock and produces an ideal output of 4745 tonnes of photoluminescent safety tiles per year. To ensure consistent output, downstream units such as solvent recovery, curing, and molding are operated continuously or semi-continuously. These must be decoupled from the batch cycle to allow stable and uninterrupted production flow throughout the year. This represents the facility's optimal capacity, assuming no unplanned interruptions.

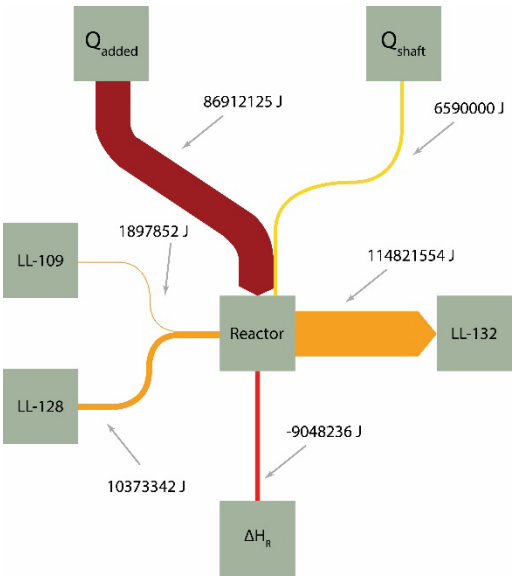

Figure 10. Schematic diagram of the reactor energy balance.

In the reactor energy balance, feed streams LL-109 and LL-128 enter at ambient temperature carrying 1.898 MJ (shredded wind-blade feedstock of glass fibers and epoxy resin) and 10.373 MJ (solvent mixture), respectively. The enthalpies of all streams were computed by integrating species-specific heat capacities from ambient to reaction temperature and adding standard enthalpies of formation. To raise the reactor contents from ambient to 90 °C, we supply 86.912 MJ of heat (Q_{added}). A scrapper agitator delivers 6.590 MJ of shaft work (Q_{shaft}), both providing the mechanical energy assumed in our ΔH calculation and preventing matrix formation on the vessel walls. These inputs, totaling approximately 105.773 MJ, exit as 114.822 MJ in outlet stream LL-132, yielding a net reaction enthalpy ΔH_R of –9.048 MJ (see Figure 10).

4. Kinetic Modeling and Reactor Analysis

4.1 Derivation of Degradation Rate from Empirical Data

The degradation of epoxy resin under microwave-assisted solvolysis using a mixture of hydrogen peroxide and acetic acid proceeds through a radical-based oxidation mechanism. The solvent system forms peracetic acid in situ via the reaction of hydrogen peroxide with acetic acid. Upon microwave irradiation, this peracetic acid decomposes to generate hydroxyl and acyloxy radicals, which initiate the cleavage of the epoxy's crosslinked network. These radicals attack the C–N and C–O bonds of the epoxy framework, fragmenting the polymer into smaller, soluble compounds.

The extent of epoxy decomposition depends primarily on the solvent composition, microwave residence time, and reaction temperature. To model this behavior, a pseudo-first-order kinetic approach is employed. It is assumed that acetic acid is used in stoichiometric or practical excess relative to hydrogen peroxide and remains approximately constant during the reaction. Thus, the rate of degradation is governed by the concentration of hydrogen peroxide, allowing a pseudo-first-order simplification. The effective oxidative strength of the solvent system is more accurately represented by the molar ratio $\varphi = [H_2O_2] / [CH_3COOH]$. This ratio governs the formation rate of peracetic acid and the availability of active radicals, rather than the absolute concentrations of each

component. Microwave heating ensures rapid energy delivery. Under proper process control, the reaction is conducted at a maintained temperature of 90°C. At this stage of modeling, temperature is assumed uniform and well-regulated. Although prior experimental work used higher microwave exposure temperatures (~183°C), industrial systems often favor moderate and safer operating conditions. The Arrhenius correction applied ensures the model reflects this lower temperature. The model assumes that the viscosity of the solvent and thermal properties of the epoxy do not change dramatically during the degradation phase. These simplifications are suitable for first-principles design and conservative process modeling. The degradation process is governed by chemical kinetics rather than mass transfer limitations, owing to the increased diffusion rate and surface permeability of the epoxy under microwave-induced swelling.

Given these assumptions, the epoxy degradation efficiency X (expressed as a fraction from 0 to 1) is modeled as a function of residence time τ (in seconds) and oxidant ratio φ as:

$$X(\tau) = 1 - \exp(-R_D * \tau) \tag{9}$$

where,

$$R_D = k_0 * \varphi \tag{10}$$

The variable k_0 represents the rate constant at 183°C. The average experimental data from a published study using was used to solve for k_0[5].

$$k_{0,183^\circ\mathrm{C}} \approx 0.0463\ \mathrm{s}^{-1} \tag{11}$$

To correct for operation at 90°C, the Arrhenius equation is applied using: E_a= 50000 J/mol (assumed as per the average value of the various samples of epoxy degradation reactions); R = 8.314 J/mol·K,

Calculated as:

$$k_0 \approx 0.00158\ \mathrm{s}^{-1} \tag{12}$$

This represents the intrinsic degradation rate constant at 90°C, adjusted to account for the slower reaction kinetics expected at this reduced temperature. Substituting into the kinetics:

$$X(\tau) = 1 - \exp(-0.00158 * \varphi * \tau) \tag{13}$$

This equation describes epoxy degradation at 90°C.

To ensure complete or near-complete degradation in an industrial setting, a residence time of 3 hours is selected. This value is practical for batch reactors. Using this τ and φ = 0.43:

$$R_D = 0.000679\ \mathrm{s}^{-1} \tag{14}$$

$$X \approx 0.9993 \quad (15)$$

This confirms that almost full epoxy degradation can be achieved, validating the selected residence time as sufficient for high-efficiency material recycling. The choice of 90°C balances energy efficiency and safety. It avoids the excessive charring, solvent evaporation, and system complexity that arise at higher temperatures. This simplified model, now corrected for temperature can be used for predicting decomposition efficiency at different oxidant compositions, performing sensitivity analysis.

4.2 Simulation of Solvolysis Batch Reactors (RE-101 - Re-104) in ChemCAD

In this study, the degradation of epoxy resin was simulated inside a vessel reactor under microwave-assisted solvolysis conditions using ChemCAD. The simulation was configured as a semi-batch vessel reactor, where all components were initially charged into the reactor, and no feed or product streams were connected during the reaction. The initial mass is for a single batch. The process was modeled isothermally at 90°C and 1 atm, with a defined residence time of 3 hours. This residence time was selected based on kinetic modeling, which indicated that complete epoxy degradation could be achieved under these conditions. The epoxy matrix was represented by the component o,p-bisphenol A. Glass fiber was included as an inert, non-reacting component to represent the reinforcement phase in composite materials. As expected, the mass of glass fiber remained constant throughout the simulation, confirming its passive behavior in the system. Acetic acid and hydrogen peroxide were introduced as reactive solvents. These components were assigned stoichiometric coefficients of both –1 and +1 to indicate their dual role in the simulation: they contributed to the reactive environment through radical generation but were not consumed overall. This representation reflects their real chemical function in generating peracetic acid and driving epoxy degradation via radical pathways. Although the default reactor model in ChemCAD uses Langmuir-Hinshelwood kinetics, this framework was overridden by implementing a custom VBA function. This VBA script replaced the standard kinetic expression with a simplified pseudo-first-order model derived from experimental data. In this model, the degradation rate was calculated using the oxidant ratio, defined as the ratio of hydrogen peroxide concentration to acetic acid concentration. The following rate expression is applied as in Equation (13).

To evaluate the sensitivity of the system to solvent composition, several simulations were conducted with varying initial amounts of hydrogen peroxide and acetic acid. The VBA model dynamically recalculated the degradation rate based on these inputs. This enabled a direct comparison of degradation performance across multiple solvent ratios.

By embedding the simplified kinetic model within ChemCAD using VBA, a dynamic and composition-sensitive simulation of epoxy degradation was achieved. The model responded to

changes in solvent ratios and allowed for efficient exploration of reaction behavior under varied conditions.

Table 1. Simulation cases with different amounts of H_2O_2 and CH_3COOH; left - Set 1: Constant H_2O_2 amount, changing CH_3COOH amounts, right - Set 2: Constant CH_3COOH amount, changing H_2O_2 amounts.

Case	φ (H_2O_2 / CH_3COOH)	Degradation (%)
1	0.71	100
2	1.03	94
3	1.41	92
4	2.10	86

Case	φ (H_2O_2 / CH_3COOH)	Degradation (%)
5	0.71	94
6	1.06	96.7
7	1.41	98.3
8	2.12	100

A comparison of the two simulation sets (see Table 1), each varying the H_2O_2/CH_3COOH molar ratio (φ), highlights the crucial difference between relative ratio and absolute quantity of reagents in determining epoxy degradation efficiency. In both sets, φ ranges from approximately 0.71 to 2.12, calculated using molar conversions from the mass data. However, the degradation outcomes diverge significantly between the two series, despite overlapping φ values. In Set 1, φ was increased by reducing the amount of acetic acid, while keeping H_2O_2 constant at 32 kg. This caused degradation to decrease steadily from 100% (φ = 0.71) to only 86% (φ = 2.10). In Set 2, φ was increased by increasing the amount of H_2O_2, with acetic acid held constant at 55 kg. Here, degradation improved consistently with φ, from 94% (φ = 0.71) to complete degradation at φ = 2.12. This divergence demonstrates that while φ (molar H_2O_2 / CH_3COOH) is a valuable kinetic descriptor, it does not fully govern degradation unless the solvent, particularly acetic acid, is present

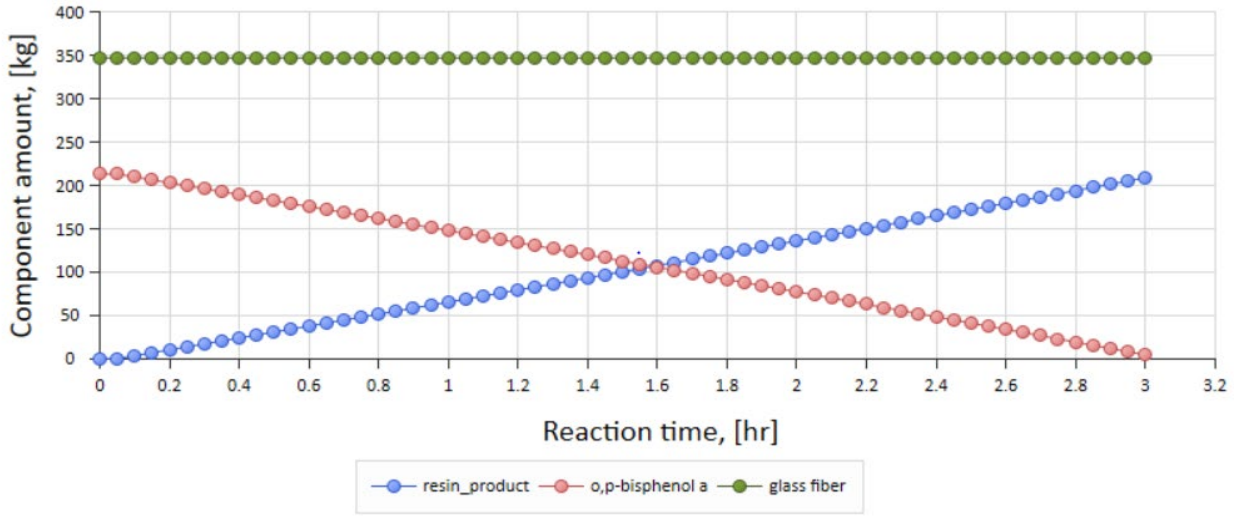

Figure 11. The result of Case 8 with nearly maximum degradation efficiency.

in sufficient excess. In Set 1, higher φ values resulted from acetic acid deficiency, leading to poor peracetic acid formation and limited free radical activity. In contrast, Set 2 maintained a consistent solvent baseline, allowing increased oxidant to translate into higher degradation rates.

If acetic acid is not in excess, increasing φ can decrease reaction performance. If acetic acid is in excess, increasing φ (by adding more H_2O_2) enhances degradation efficiency. This underscores a key design insight: absolute reagent availability matters. Efficient epoxy solvolysis requires not just the right ratio, but also enough molar mass of each reactant to maintain active species throughout the residence time.

ChemCAD illustrates (see Figure 11) where the near maximum degradation can be achieved with Case 8. The final mass amount of the reactant (added to the component list as o,p-bisphenol a) reaches zero at the end of the residence time.

The oxidant ratio φ provides a useful optimization tool, but only when acetic acid is in sufficient excess. If CH_3COOH is too low, increasing φ by reducing solvent actually decreases degradation efficiency, since peracetic acid formation is limited. Therefore, optimization should not focus on maximizing φ alone, but on ensuring adequate solvent availability first. Once CH_3COOH is non-limiting, φ can be effectively tuned, preferably by increasing H_2O_2, to enhance performance. An optimal φ range of ~1.0-1.4, with enough solvent present, offers the best balance between degradation efficiency and reagent use. While this behavior may not appear critical in highly reactive lab-scale conditions, it becomes especially relevant in industrial systems, where degradation rates are typically lower due to mass transfer limits and scale. In such cases, the insights from this study can lead to significant performance improvements.

5. Cost Estimation

5.1 Capital Expenditure

Capital expenditure (CapEx) includes all the initial costs needed to build and prepare the plant for operation. This covers the purchase of equipment such as the batch reactor, shredder, pumps, tanks, and other supporting units. Equipment costs were estimated based on standard references [14], [15] and capacity adjustments were made using the commonly applied six-tenths scaling rule:

$$C_2 = C_1 * \left(\frac{Capacity_2}{Capacity_1}\right)^{0.6} \quad (16)$$

Where C_1 is the known cost for $capacity_1$, C_2 is the scaled cost for required capacity ($capacity_2$), and 0.6 is the scaling exponent.

In addition to equipment cost which is €1,046,000, there are installation and construction expenses like piping, electrical systems, control units, insulation, and civil works. Civil work is the largest portion of this, estimated at €10.5 million. Together, all direct installation costs amount to approximately €11.5 million.

There are also indirect costs such as engineering, supervision, construction overhead, and commissioning. These are calculated as a proportion of the direct costs and total around €314,000. Land acquisition is based on 30,000 m² at €350 per m². The final total capital investment is calculated as €23,353,930, which includes all these components.

5.2 Operational Expenditure

Operational costs (OpEx) cover all recurring expenses required to keep the plant running efficiently each year. These include the consumption of utilities such as electricity, cooling water, and drinking water, along with wastewater disposal services. A significant portion of the costs is also attributed to raw materials, including acetic acid, hydrogen peroxide, and various additives used in the process.

Labor expenses are calculated based on 100 employees, including operating staff and supervisory roles, while maintenance costs are estimated as 4% of the total capital investment. Additional yearly expenses such as transport, insurance, and planned equipment replacements are also included in the operating cost estimates. Over the years, these operational costs gradually increase due to inflation, and the values are adjusted using appropriate indices for labor, energy, maintenance, and materials to reflect realistic cost development over time.

5.3 Cumulative Cash Flow (CCF)

Cumulative cash flow (CCF) is used to evaluate the long-term financial performance of the plant by summing up the yearly net cash flows (NCF). Each year's net cash flow is calculated as the difference between product income and the total of operational and capital expenses. The cumulative value shows how much money the project has gained or lost up to a given point in time. This is calculated using the following equation:

$$NCF = Product\ Income - (CapEx + OpEx) \tag{17}$$

$$CCF = \sum_{t_0}^{t} NCF \tag{18}$$

In the first year, the project shows a large negative value due to the one-time capital investment. Starting from 2030, after production begins, the plant starts generating income. As operating costs remain relatively stable and revenue increases, the yearly net cash flow becomes positive. These positive yearly results build up over time, reducing the initial deficit and eventually turning the cumulative cash flow into positive territory.

The Net Cash Flow (NCF) graph (see Figure 11) reflects this transition clearly. It shows a sharp negative value in the first year due to CapEx, followed by steady and growing positive cash flows from 2030 onwards. The rise in NCF is mainly driven by consistent product sales and moderate growth in operating costs.

The Cumulative Cash Flow graph (see Figure 12) shows the point where the initial investment is fully recovered. This breakeven occurs in 2033, four years after production starts. This means the payback time of the project is approximately four years, which is considered reasonable for an industrial-scale investment. Beyond this point, the project maintains a positive financial trajectory, with annual profits showing consistent growth. The upward trend in both the NCF and CCF graphs confirms that the project is not only financially viable but also capable of generating long-term returns.

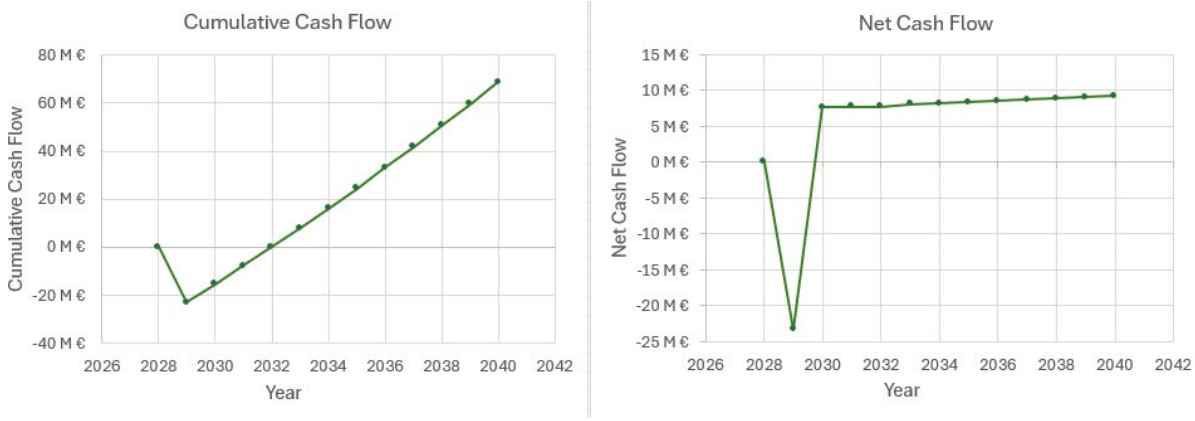

Figure 12. Cumulative (left) and Net Cash Flow (right)

5.4 Net Present Value

Net Present Value (NPV) is a core financial metric used to assess the profitability of investment projects. It represents the difference between the present value of future cash inflows and the present value of cash outflows over the lifetime of a project. By discounting future earnings, NPV accounts for the time value of money, ensuring that delayed returns are properly weighed against initial and ongoing costs. A positive NPV indicates that the project is expected to create a net economic value.

The NPV is calculated using the following equation:

$$NPV = \sum_{t_0}^{t} \frac{NCF}{(1+i)^t} \tag{19}$$

where NCF is the net cash flow in year t_0 , i is the discount rate, and t is the total project duration in years. Figure 13 illustrates the evolution of NPV from 2028 to 2040. After the investment phase, the curve rises steeply, indicating the start of significant revenue generation and net positive cash flows. This upward trend continues until the peak in 2030, which corresponds to the period of maximum financial return.

In the following years, a gradual decline in NPV is observed. This trend can be attributed not only to the natural discounting of future revenues but also to potential shifts in the competitive landscape. As more companies enter the market and offer similar products or technologies, the resulting competition may reduce our market share or force down prices. These effects decrease future cash flows and are reflected in the diminishing NPV over time. Nevertheless, the NPV remains positive throughout the entire project horizon, confirming that the investment is economically viable under the current assumptions.

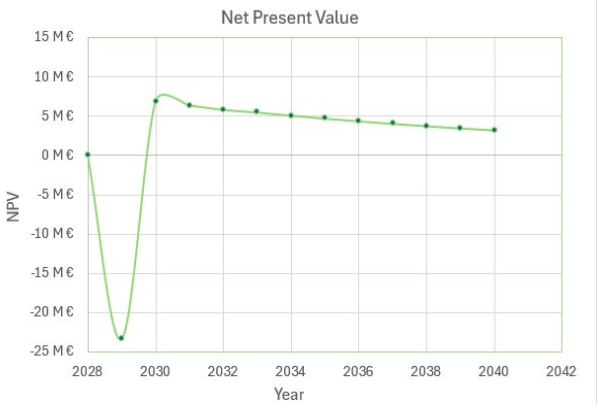

Figure 13. Net Present Value.

5.5 Internal Rate of Return

In addition to NPV, the Internal Rate of Return (IRR) was calculated to further assess the project's profitability. IRR is the discount rate at which the NPV becomes zero, representing the break-even return for the investment:

$$0 = \sum_{t_0}^{t} \frac{NCF}{(1 + IRR)^t} \tag{20}$$

Based on the actual yearly net cash flows from 2029 to 2040 and an initial investment of €23.35 million, the IRR was computed to be approximately 18.2%. This is significantly higher than the assumed discount rate of 8%, confirming the project's financial viability and its ability to generate returns well above its cost of capital.

6. Process Safety

This bow tie diagram (see Figure 14) illustrates the risk management of thermal runaway in a solvolysis reactor. Key causes such as uneven microwave absorption and blocked vents are controlled through preventive measures like dielectric scans and smart dosing. On the mitigation side, consequences like operator exposure and vapor release are addressed with safeguards such as PPE protocols, Faraday shielding, and pressure relief systems. The diagram highlights a balanced approach of prevention and mitigation to ensure reactor safety.

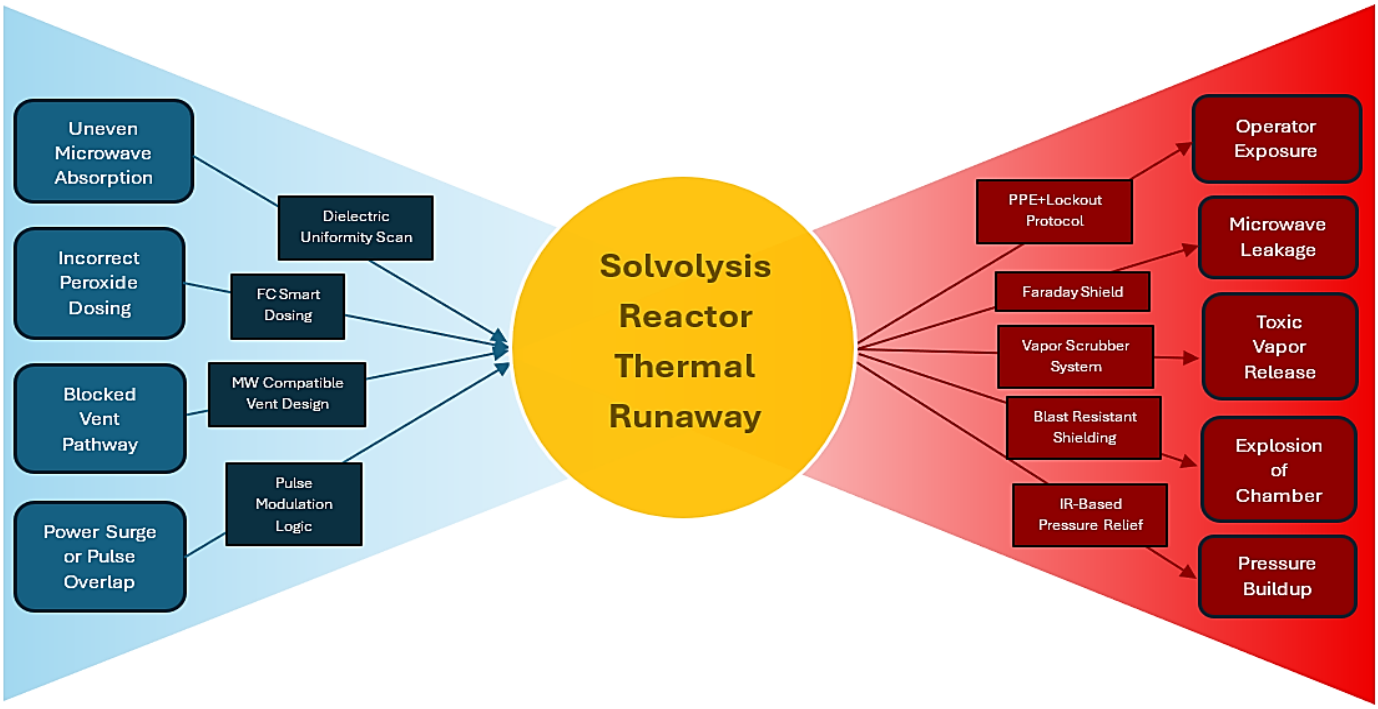

Figure 14. Bow - Tie diagram for thermal runaway in solvolysis reactor.

7. Environmental Analysis

The carbon footprint assessment provides insight into the environmental impact of each recycling method by quantifying their greenhouse gas emissions across Scopes 1, 2, and 3 (see Table 2). Scope 1 includes direct emissions from process activities, Scope 2 covers emissions from electricity use, and Scope 3 accounts for indirect sources such as transportation, packaging, and material production.

Incineration leads to the highest emissions, with Scope 1 alone exceeding 7000 tCO_2e due to combustion of fiber and resin. Pyrolysis also results in considerable direct emissions through high-temperature decomposition of composite materials. Although landfilling appears to produce minimal emissions, its footprint is mainly due to transport and packaging (Scope 3).

Solvolysis, by contrast, presents a significantly lower carbon footprint. Most emissions fall under Scope 1, primarily from the use of acetic acid and hydrogen peroxide. Scope 3 emissions amount to approximately 304.76 tCO_2e, stemming from indirect activities linked to the process. Crucially, electricity used in solvolysis is sourced from renewable energy, resulting in zero Scope 2 emissions. This method avoids combustion and operates under milder conditions, which helps preserve

material quality and reduce greenhouse gas emissions, making it a more sustainable and circular solution for wind turbine blade recycling.

Table 2. Carbon Footprint of Different Technologies.

Scope	Solvolysis	Landfilling	Incineration	Pyrolysis
	tCO2e			
Scope 1	1204.80	0.00	7130.20	2100.00
Scope 2	0.00	0.00	0.00	62.40
Scope 3	304.76	65.90	66.90	6.70
Total	1509.56	65.90	7197.10	2169.10

8. Market Analysis and Commercialization Strategy

The marketing strategy centers on two safety products: photoluminescent safety tiles and rubber-based textured floor blocks. The feedstock is sourced from decommissioned blades supplied primarily by Siemens Gamesa (52%) and Vestas (48%), providing an input of glass fiber-reinforced thermoset material, which forms the structural base of both products.

The photoluminescent tiles are designed specifically for use in emergency escape paths where conventional electric lighting poses a significant ignition hazard. In environments where flammable gases or volatile chemicals may be present, electrostatic discharge from wiring or fixtures can serve as an ignition source, further escalating an incident. These tiles absorb ambient light and emit it in darkness, eliminating the need for powered systems while ensuring continuous visibility during critical evacuation scenarios. Their application aligns with ATEX safety protocols and supports compliance in facilities operating under high-risk process conditions. The textured floor blocks, developed using a mixture of shredded blade fibers and elastomeric fillers, are targeted at plant walkways and access corridors. Their composition is developed for

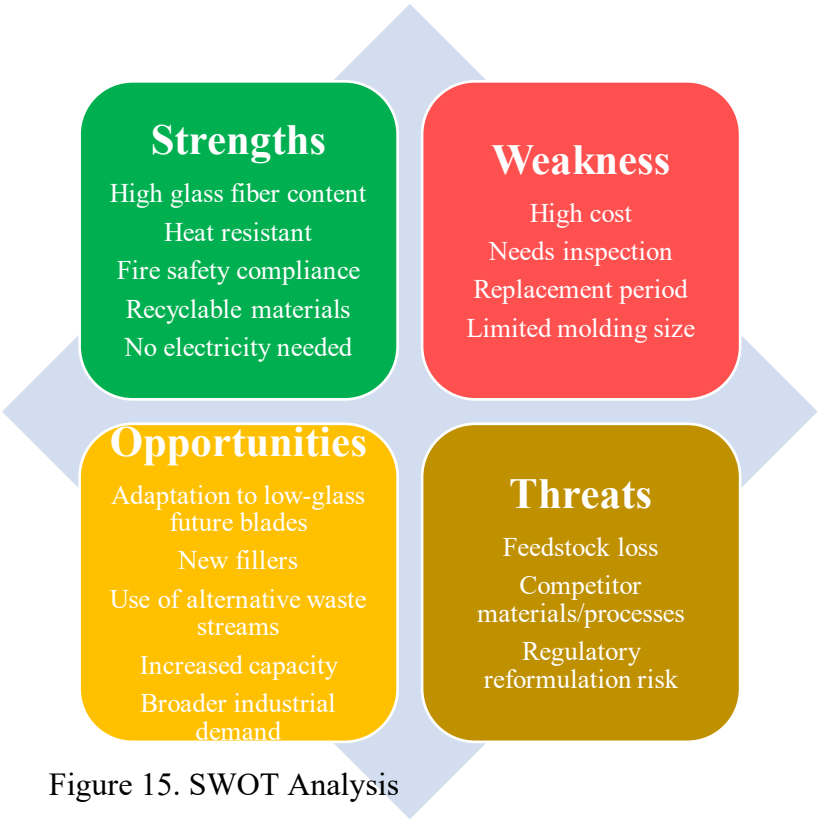

Figure 15. SWOT Analysis

thermal stability, mechanical durability, and slip resistance under wet or contaminated surface conditions. The elevated glass fiber content provides improved load-bearing capacity and flame retardancy compared to traditional polymer-only solutions. These blocks support safe personnel movement within industrial facilities and are particularly well-suited for operational areas.

From a cost perspective, both products are more expensive than conventional safety flooring or photoluminescent paint. This is due to the high-quality of the products. However, these products offer measurable operational benefits: they reduce maintenance frequency, meet fire safety classifications, and support environmental impact reduction targets by using end-of-life composite waste.

The target market includes chemical plants, refineries, power generation facilities, offshore structures, gas terminals and similar industrial environments with elevated safety requirements.

The technical strengths of the products lie in their high glass fiber content, which contributes to increased heat resistance, structural integrity, and dimensional stability under load. Additionally, the base materials are recyclable, aligning with emerging regulatory standards in sustainable industrial design (see Figure 16).

However, there are inherent limitations. The product cost remains relatively high, and the products require periodic inspection and replacement intervals estimated at 5–12 years. The dimensions of the final products are also restricted by client infrastructure and mold specifications, limiting design flexibility.

Looking forward, there is an opportunity to adjust formulations based on the evolving characteristics of recyclable blade materials. New-generation wind turbine blades will likely contain lower glass fiber ratios, necessitating the incorporation of additional fillers such as polymers, mineral additives, or industrial by-products to maintain mechanical performance. This also creates room for increased production throughput and material diversity, particularly in the rubber block line, where non-fibrous fillers may be viable.

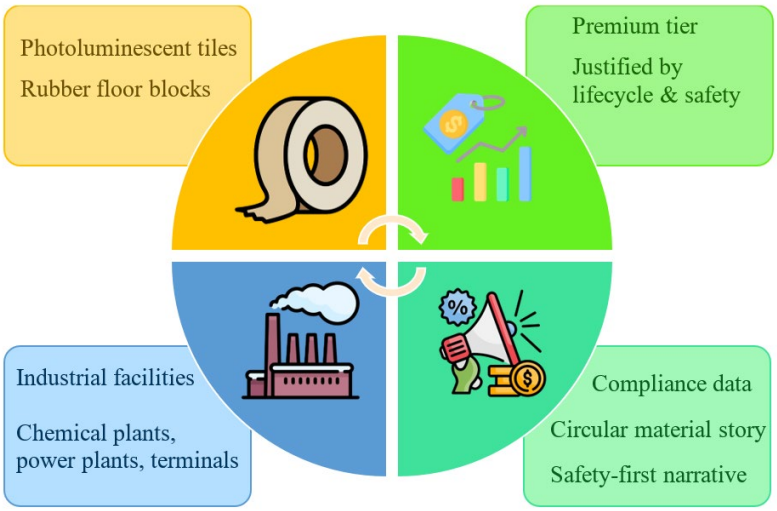

Figure 16. 4 Ps of Marketing

On the risk side, feedstock availability could be affected if blade manufacturing corporates such as Siemens or Vestas begin internalizing blade recycling operations, reducing third-party access to waste material. Regulatory pressure from the EU, particularly related to chemical safety and microplastic legislation, may result in the restriction of certain additives or

processing methods, requiring constant readiness to adapt. Finally, the emergence of competitive recycling technologies or alternative materials could impact on both the market share and pricing dynamics of the current offerings. The strategy moving forward involves reinforcing the product's scientific and safety credentials, integrating performance data into technical documentation, and maintaining flexibility in material sourcing and product formulation to respond to future regulatory and supply-side changes. The central value proposition remains: transforming high-performance industrial waste into functionally critical safety products, without compromising on operational reliability or compliance (see Figure 17).

9. Summary

This study presents a high-efficiency, low-emission approach to recycling glass fiber-reinforced wind turbine blades through microwave-assisted green solvolysis to produce photoluminescent tiles for emergency visibility and rubber floor blocks for slip-resistant, durable walkways. By generating peracetic acid in situ from hydrogen peroxide and acetic acid, the process enables radical-driven degradation of the epoxy matrix at 90 °C, achieving nearly full conversion while preserving the structural integrity of embedded glass fibers. The process design, executed in a semi-batch configuration with four modular reactors, enables the annual treatment of 4438 tonnes of GFRP feedstock, yielding approximately 4745 tonnes of products.

Economically, the process is based on a €23.35 million capital investment, reaching payback in 4 years and delivering an internal rate of return of 18.2%. Compared to conventional recycling or disposal methods such as pyrolysis or incineration, microwave-assisted solvolysis emits only low amounts of the carbon dioxide equivalents, making it not only a cleaner but more resource-efficient solution. It directly supports EU circular economy directives by reintegrating high-value materials into essential applications rather than downcycling or landfilling them.

The impact goes beyond efficiency or emissions metrics, it transforms waste into safety itself. The recovered materials are developed into infrastructure that protects lives during emergencies, providing illumination and stability in the most demanding conditions. In this way, the process delivers on both ecological and human value.

It is not just a recycling solution, it is a reinvention of waste into resilience. With the glow that guides and the clarion that saves, Glarion lights the way to safety.

Literature

[1] F. Spini and P. Bettini, "End-of-Life wind turbine blades: Review on recycling strategies," *Compos. Part B Eng.*, vol. 275, p. 111290, Apr. 2024, doi: 10.1016/j.compositesb.2024.111290.

[2] "The Construction Specifier," Construction Specifier. Accessed: May 23, 2025. [Online]. Available: https://www.constructionspecifier.com/

[3] "(PDF) High Performance Flooring Materials from Recycled Rubber." Accessed: July 22, 2025. [Online]. Available: https://www.researchgate.net/publication/326522359_High_Performance_Flooring_Materials_from_Recycled_Rubber

[4] G. Oliveux, L. O. Dandy, and G. A. Leeke, "Degradation of a model epoxy resin by solvolysis routes," *Polym. Degrad. Stab.*, vol. 118, pp. 96–103, Aug. 2015, doi: 10.1016/j.polymdegradstab.2015.04.016.

[5] M. Rani, P. Choudhary, V. Krishnan, and S. Zafar, "Development of sustainable microwave-based approach to recover glass fibers for wind turbine blades composite waste," *Resour. Conserv. Recycl.*, vol. 179, p. 106107, Apr. 2022, doi: 10.1016/j.resconrec.2021.106107.

[6] S. Dąbrowska, T. Chudoba, J. Wojnarowicz, and W. Łojkowski, "Current Trends in the Development of Microwave Reactors for the Synthesis of Nanomaterials in Laboratories and Industries: A Review," *Crystals*, vol. 8, no. 10, Art. no. 10, Sept. 2018, doi: 10.3390/cryst8100379.

[7] P. Johst, M. Bühl, C. Enderle, R. Kupfer, N. Modler, and R. Böhm, "Forecasting wind turbine blade waste with material composition and geographical distribution: Methodology and application to Germany," *Resour. Conserv. Recycl.*, vol. 211, p. 107876, Dec. 2024, doi: 10.1016/j.resconrec.2024.107876.

[8] S. Dattilo, G. Cicala, P. M. Riccobene, C. Puglisi, and L. Saitta, "Full Recycling and Re-Use of Bio-Based Epoxy Thermosets: Chemical and Thermomechanical Characterization of the Recycled Matrices," *Polymers*, vol. 14, no. 22, p. 4828, Nov. 2022, doi: 10.3390/polym14224828.

[9] X. Li, J. Zhang, L. Zhang, A. R. de Luzuriaga, A. Rekondo, and D.-Y. Wang, "Recyclable flame-retardant epoxy composites based on disulfide bonds. Flammability and recyclability," *Compos. Commun.*, vol. 25, p. 100754, June 2021, doi: 10.1016/j.coco.2021.100754.

[10] A. M. Binyaseen *et al.*, "Development of epoxy/rice straw-based cellulose nanowhiskers composite smart coating immobilized with rare-earth doped aluminate: Photoluminescence and anticorrosion properties for sustainability," *Ceram. Int.*, vol. 48, no. 4, pp. 4841–4850, Feb. 2022, doi: 10.1016/j.ceramint.2021.11.020.

[11] Jasonxue, "Hindered Amine Light Stabilizer: Protecting Polymers from Degradation," Wellt. Accessed: July 22, 2025. [Online]. Available: https://welltchemicals.com/blog/hindered-amine-light-stabilizer/

[12] K. J. Geretschläger, G. M. Wallner, I. Hintersteiner, and W. Buchberger, "Damp Heat Aging Behavior of a Polyamide-Based Backsheet for Photovoltaic Modules," *J. Sol. Energy Eng.*, vol. 138, no. 041003, Apr. 2016, doi: 10.1115/1.4032977.

[13] P. Kiss, W. Stadlbauer, C. Burgstaller, and V.-M. Archodoulaki, "Development of high-performance glass fibre-polypropylene composite laminates: Effect of fibre sizing type and coupling agent concentration on mechanical properties," *Compos. Part Appl. Sci. Manuf.*, vol. 138, p. 106056, Nov. 2020, doi: 10.1016/j.compositesa.2020.106056.

[14] J. J. Carberry, J. R. Fair, W. P. Schowalter, M. Tipell, J. Wei, and M. S. Peters, “McGraw-Hill Chemical Engineering Series”.
[15] R. Turton, Ed., *Analysis, synthesis, and design of chemical processes*, 3rd ed. in Prentice Hall PTR international series in the physical and chemical engineering sciences. Upper Saddle River, N.J: Prentice Hall, 2009.